Unlike the case for the planar box considered at the beginning of this section, the pair collision time $t_{\rm pair}$ is generally finite: even two particles moving apart from each other eventually collide, after winding several times around the simulation box (see Fig. 2.12), although this is relevant only for low-density systems. We have to decide on a good strategy to cope with this: either carefully program the situation in Fig. 2.12, or stay with our initial attitude (in Alg. 2.2 (`pair-time`)) that particles moving away from each other never collide—a dangerous fudge that must be remembered when we are running the program for a few small disks in a large box.

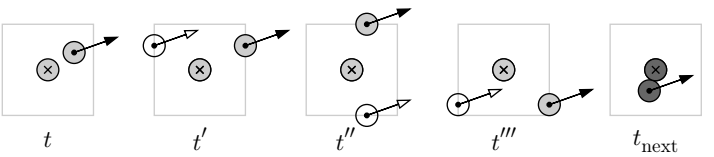

Fig. 2.12 Pair collision in a box with periodic boundary conditions.

The complications of Fig. 2.12 are also absent in Sinai's system of two relatively large disks in a small periodic box, such that disks cannot pass by each other (Sinai, 1970). Figure 2.13 shows event frames generated by Alg. 2.1 (`event-disks`), using the (noninertial) stationary-disk reference frame that was introduced in Fig. 2.6. Sinai's hard disks can be simulated

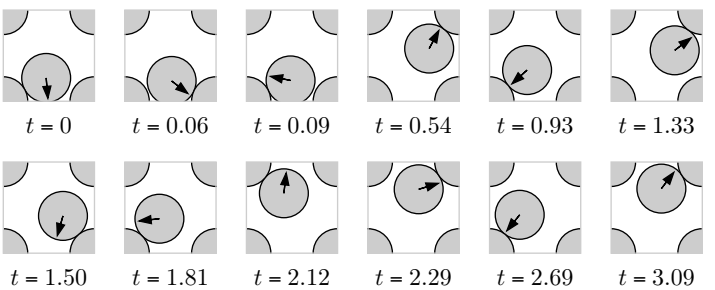

Fig. 2.13 Time evolution of two disks in a square box with periodic boundary conditions, in the stationary-disk reference frame.

directly as a single point in the stationary-disk reference frame.

2.2 Boltzmann's statistical mechanics

We could set up the event-driven algorithm of Section 2.1 in a few hours and follow the ballet of disks (spheres) approaching and flying away from each other along intricate, even unpredictable trajectories. In doing so,

however, we engage in a computational project which in many respects is far too complicated. In the limit $t \to \infty$, detailed timing information, for example the ordering of the snapshots in Fig. 2.8, does not enter into the density profiles, spatial correlation functions, thermodynamic properties, etc. We need to know only how often a configuration a appears during an infinitely long molecular dynamics calculation. For hard spheres, it is the quintessence of Boltzmann's statistical mechanics that any two legal configurations a and b have the same probability to appear: $\pi(a) = \pi(b)$ (see Fig. 2.14).

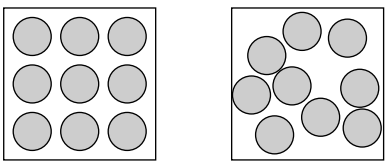

Fig. 2.14 Equiprobability principle for hard disks: $\pi(a) = \pi(b)$.

More precisely (for an infinitely long simulation), this means the following:

$$\left\{ \begin{array}{c} \text{probability of configuration with} \\ [\mathbf{x}_1, \mathbf{x}_1 + \mathrm{d}\mathbf{x}_1], \ldots, [\mathbf{x}_N, \mathbf{x}_N + \mathrm{d}\mathbf{x}_N] \end{array} \right\} \propto \pi(\mathbf{x}_1, \ldots, \mathbf{x}_N)\, \mathrm{d}\mathbf{x}_1, \ldots, \mathrm{d}\mathbf{x}_N,$$

where

$$\pi(\mathbf{x}_1, \ldots, \mathbf{x}_N) = \begin{cases} 1 & \text{if configuration legal} \\ 0 & \text{otherwise} \end{cases} . \tag{2.5}$$

In the presence of an energy E which contains kinetic and potential terms, eqn (2.5) takes the form of the equiprobability principle $\pi(a) = \pi(E(a))$, where a refers to positions and velocities (see Subsection 2.2.4). In the hard-sphere model, the potential energy vanishes for all legal configurations, and we get back to eqn (2.5). This hypothesis can be illustrated by molecular dynamics simulations (see Fig. 2.15), but the equal probability of all configurations a and b is an axiom in statistical mechanics, and does not follow from simple principles, such as microreversibility or detailed balance. Its verification from outside of statistical mechanics, by solving Newton's equations of motion, has presented a formidable mathematical challenge. Modern research in mathematics has gone far in actually proving ergodicity, the equivalence between Newton's deterministic mechanics and Boltzmann's statistical mechanics, for the special case of hard spheres. The first milestone result of Sinai (1970), a 50-page proof, shows rigorously that the two-disk problem of Fig. 2.13 is ergodic. Several decades later it has become possible to prove that general hard-disk and hard-sphere systems are indeed ergodic, under very mild assumptions (Simanyi 2003, 2004).

Fig. 2.15 Trajectory of the system shown in Fig. 2.13 after 18, 50, and 500 collisions.

Besides the mathematically rigorous approach, many excellent arguments plead in favor of the equiprobability principle, for hard spheres in particular, and for statistical physical systems in general. One of the most discussed is Jaynes' information-theoretical principle, which essentially states (for hard spheres) that the equal-probability choice is an unbiased guess. In Fig. 2.15, we show the trajectory of Sinai's two-disk system in the stationary-disk reference frame. It has been mathematically proven that for almost all initial conditions, the central area is swept out evenly. This is the simplest pattern, the one containing the least information about the system, and the one corresponding to Jaynes' principle. The latter principle is closely related to Bayesian statistics (see Subsection 1.3.4), with a most interesting difference. In Bayesian statistics, one is hampered by the arbitrariness of defining an unbiased (flat) a priori probability: what is flat with a given choice of variables acquires structure under a coordinate transformation. In physics, the problem can be avoided because there exists a special coordinate system—Cartesian positions and velocities. Boltzmann's equal-probability choice is to be understood with respect to Cartesian coordinates, as indicated in eqn (2.5).

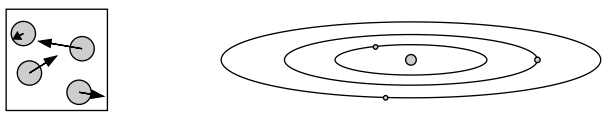

Fig. 2.16 Hard disks (*left*) and planets orbiting the sun (*right*): classical dynamic systems with greatly different behavior.

The foundations of statistical mechanics would be simpler if all physical systems (finite or infinite, with an arbitrary energy) fell under the reign of equiprobability (eqn (2.5)) and its generalizations. However, this is not the case. A notorious counterexample to equal probability of states with equal energy is the weakly interacting system of a few planets of mass m orbiting the sun, of mass M (see Fig. 2.16). If we neglect the planet–planet interactions altogether, in the limit $m/M \to 0$, the planets orbit the sun on classical Kepler ellipses, the solutions of the two-body problem of classical mechanics. Small planet–planet interactions modify the trajectories only slightly, even in the limit of infinite times, as was shown by the seminal Kolmogorov–Arnold–Moser theorem (see Thirring (1978) for a rigorous textbook discussion). As a consequence, for small planet masses, the trajectories remain close to the unperturbed trajectories. This is totally different from what happens for small disks in a box, which usually fly off on chaotic trajectories after a few violent collisions. Statistical mechanics applies, however, for a large number of bodies (e.g. for describing a galaxy).

2.2.1 Direct disk sampling

Boltzmann's statistical mechanics calls for all legal configurations to be generated with the same statistical weight. This can be put into practice by generating all configurations—legal and illegal—with the same probability, and then throwing away (rejecting) the illegal ones. What remains are hard-disk configurations, and they are clearly generated with equal probability (see Alg. 2.7 (`direct-disks`) and Fig. 2.17). It is wasteful to bring up illegal configurations only to throw them away later, but a better solution has not yet been found. The direct-sampling algorithm can

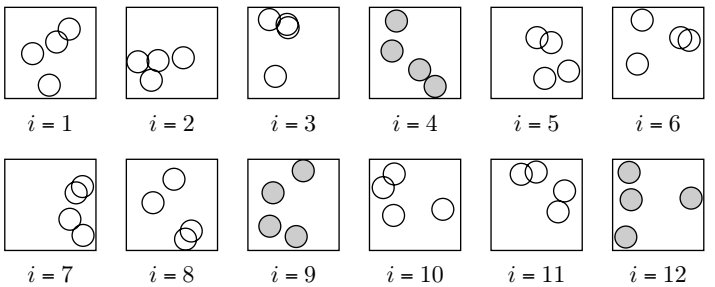

Fig. 2.17 Direct sampling for four hard disks in a box. The frames $i = 4, 9, 12$ contain legal configurations (from Alg. 2.7 (`direct-disks`)).

procedure `direct-disks`
1 **for** $k = 1, \ldots, N$ **do**
  $x_k \leftarrow \texttt{ran}\,(x_{\min}, x_{\max})$
  $y_k \leftarrow \texttt{ran}\,(y_{\min}, y_{\max})$
  for $l = 1, \ldots, k-1$ **do**
    { **if** $(\texttt{dist}\,(\mathbf{x}_k, \mathbf{x}_l) < 2\sigma)$ **goto** 1 (reject sample—tabula rasa)
output $\{\mathbf{x}_1, \ldots, \mathbf{x}_N\}$

Algorithm 2.7 `direct-disks`. Direct sampling for N disks of radius σ in a fixed box. The values of $\{x_{\min}, x_{\max}\}$, etc., depend on the system.

be written much faster than the molecular dynamics routine (Alg. 2.1 (`event-disks`)), as we need not worry about scalar products, collision subroutines etc. The output configurations $\{\mathbf{x}_1, \ldots, \mathbf{x}_N\}$ are produced with the same probability as the snapshots of Alg. 2.1 (`event-disks`) and lead to the same histograms as in Fig. 2.9 (because the physical system is ergodic). We get a flavor of the conceptual and calculational simplifications brought about by statistical mechanics.

The tabula-rasa rejection in Alg. 2.7 (`direct-disks`) often leads to confusion: instead of sweeping away the whole configuration after the generation of an overlap, one may be tempted to lift up the offending disk only, and try again (see Fig. 2.18). In this procedure of random

sequential deposition, any correctly placed disk stays put, whereas incorrectly positioned disks are moved away.

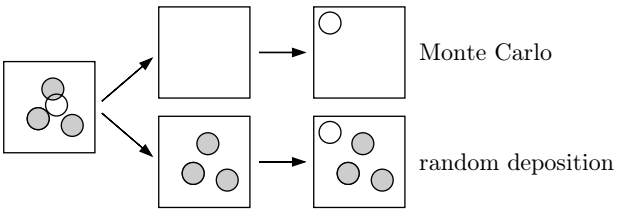

Fig. 2.18 Difference between the direct-sampling Monte Carlo method and random sequential deposition.

Random sequential deposition is an important model for adhesion and catalysis (see the discussion in Chapter 7) but not for equilibrium: all configurations are not equally probable. A simplified one-dimensional discrete hard-rod model allows us to compute deposition probabilities explicitly and show that they are not the same (see Fig. 2.19): we suppose that rods may be deposited onto five sites, with a minimum distance of three sites between them. After placing the first rod (with the same probability on all sites), we try again and again until a two-rod configuration without overlap is found.

The configurations a and b are thus generated with half the probability of their parent, whereas the configuration c, a unique descendant, inherits all the probability of its parent. We obtain

$$\pi(a) = \pi(b) = \pi(e) = \pi(f) = \frac{1}{4} \times \frac{1}{2} = \frac{1}{8},$$

whereas the configurations c and d have a probability

$$\pi(c) = \pi(d) = \frac{1}{4}.$$

In Fig. 2.19, we distinguish rods according to when they were placed (a is different from d), but the deposition probabilities are nonequivalent even if we identify a with d, b with e, and c with f. The counterexample of Fig. 2.19 proves that random deposition is incorrect for hard disks and spheres in any dimensionality, if the aim is to generate configurations with equal probabilities.

The direct-sampling Monte Carlo algorithm, as discussed before, generates all 25 legal and illegal configurations with probability 1/25. Only the six configurations $\{a, \ldots, f\}$ escape rejection, and their probabilities are $\pi(a) = \cdots = \pi(f) = 1/6$.

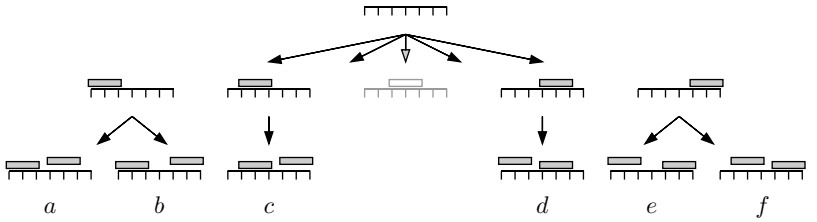

Fig. 2.19 Random deposition of discrete hard rods.

2.2.2 Partition function for hard disks

Direct sampling would solve the simulation problem for disks and spheres if its high rejection rate did not make it impractical for all but the smallest and least dense systems. To convey how serious a problem the rejections become, we show in Fig. 2.20 the configurations, of which there are only six, returned by one million trials of Alg. 2.7 (`direct-disks`) with $N = 16$ particles and a density $\eta = \pi\sigma^2 N/V = 0.3$. The acceptance rate is next to zero. It deteriorates further with increasing particle number or density.

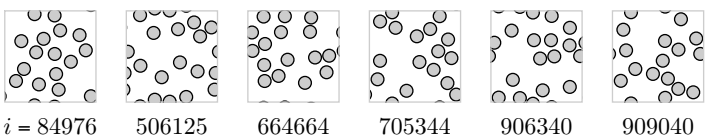

Fig. 2.20 The six survivors from 10^6 trials of Alg. 2.7 (`direct-disks`) ($N = 16$, $\eta = 0.3$, periodic boundary conditions).

Although Alg. 2.7 (`direct-disks`) does not appear to be a very useful program, we shall treat it as a VIP[3]and continue analyzing it. We shall come across a profound link between computation and physics: the acceptance rate of the algorithm is proportional to the partition function, the number of configurations of disks with a finite radius.

We could compute the acceptance rate of the direct-sampling algorithm from long runs at many different values of the radius σ, but it is better to realize that each sample of random positions $\{\mathbf{x}_1, \ldots, \mathbf{x}_N\}$ gives a hard-disk configuration for all disk radii from zero up to half the minimum distance between the vectors or for all densities smaller than a limiting $\eta_{\max}$ (we consider periodic boundary conditions; see Alg. 2.8 (`direct-disks-any`)). Running this algorithm a few million times gives the probability distribution $\pi(\eta_{\max})$ and the acceptance rate of Alg. 2.7

[3]VIP: Very Important Program.

(`direct-disks`) for all densities (see Fig. 2.21):

$$\underbrace{p_{\text{accept}}(\eta)}_{\substack{\text{acceptance rate of}\\ \text{Alg. 2.7 (direct-disks)}}} = 1 - \underbrace{\int_0^\eta \mathrm{d}\eta_{\max}\, \pi(\eta_{\max})}_{\substack{\text{integrated histogram}\\ \text{of Alg. 2.8 (direct-disks-any)}}} . \tag{2.6}$$

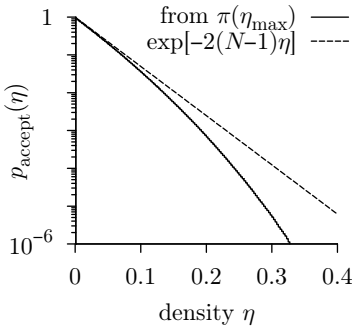

Fig. 2.21 Acceptance rate of Alg. 2.7 (`direct-disks`) for 16 disks in a square box (from Alg. 2.8 (`direct-disks-any`), using eqn (2.6)).

procedure `direct-disks-any`
input $\{N, L_x, L_y\}$
for $k = 1, \ldots, N$ **do**
$\left\{ \begin{array}{l} x_k \leftarrow \texttt{ran}\,(0, L_x) \\ y_k \leftarrow \texttt{ran}\,(0, L_y) \end{array} \right.$
$\sigma \leftarrow \frac{1}{2} \min_{k \neq l} [\texttt{dist}\,(\mathbf{x}_k, \mathbf{x}_l)]$
$\eta_{\max} \leftarrow \pi\sigma^2 N/(L_x L_y)$ (limiting density)
output $\eta_{\max}$

Algorithm 2.8 `direct-disks-any`. The limiting hard-disk density for N random vectors in an $L_x \times L_y$ box with periodic boundary conditions.

The acceptance rate is connected to the number of configurations, that is, the partition function $Z(\eta)$ for disks of covering density η. For zero radius, that is, for an ideal gas, we have

$$\left\{ \begin{array}{c} \text{number of} \\ \text{configurations} \\ \text{for density 0} \end{array} \right\} : Z(\eta = 0) = \int \mathrm{d}\mathbf{x}_1 \ldots \int \mathrm{d}\mathbf{x}_N \; = V^N.$$

The partition function $Z(\eta)$ for disks with a finite radius and a density η is related to $Z(0)$ via

$$\left\{ \begin{array}{c} \text{number of} \\ \text{configurations} \\ \text{for density } \eta \end{array} \right\} : Z(\eta) = \int \ldots \int \mathrm{d}\mathbf{x}_1 \ldots \mathrm{d}\mathbf{x}_N \; \underbrace{\pi(\mathbf{x}_1, \ldots, \mathbf{x}_N)}_{\text{for disks of finite radius}}$$
$$= Z(0) p_{\text{accept}}(\eta).$$

This expression resembles eqn (1.38), where the volume of the unit sphere in d dimensions was related to the volume of a hypercube via the acceptance rate of a direct-sampling algorithm.

We shall now determine $p_{\text{accept}}(\eta)$ for the hard-disk system, and its partition function, for small densities η in a box with periodic boundary conditions, using a basic concept in statistical physics, the virial expansion. Clearly,

$$Z(\eta) = \int \ldots \int \mathrm{d}\mathbf{x}_1 \ldots \mathrm{d}\mathbf{x}_N \underbrace{[1 - \Upsilon(\mathbf{x}_1, \mathbf{x}_2)]}_{\substack{\text{no overlap}\\ \text{between 1 and 2}}} [1 - \Upsilon(\mathbf{x}_1, \mathbf{x}_3)] \cdots [1 - \Upsilon(\mathbf{x}_{N-1}, \mathbf{x}_N)], \tag{2.7}$$

where

$$\Upsilon(\mathbf{x}_k, \mathbf{x}_l) = \begin{cases} 1 & \text{if } \mathrm{dist}(\mathbf{x}_k, \mathbf{x}_l) < 2\sigma \\ 0 & \text{otherwise} \end{cases}.$$

The product in eqn (2.7) can be multiplied out. The dominant term collects a "1" in each of the $N(N-1)/2$ parentheses, the next largest term (for small σ) picks up a single term $\Upsilon(\mathbf{x}_k, \mathbf{x}_l)$, etc. Because

$$\int\int \mathrm{d}\mathbf{x}_k \, \mathrm{d}\mathbf{x}_l \; \Upsilon(\mathbf{x}_k, \mathbf{x}_l) = V \underbrace{\int \mathrm{d}\mathbf{x}_l \; \Upsilon(\mathbf{x}_k, \mathbf{x}_l)}_{\substack{\text{volume of} \\ \text{excluded region for } \mathbf{x}_l}} = V^2 \cdot 4\pi\frac{\sigma^2}{V},$$

(the area of a disk of radius 2σ appears; see Fig. 2.22), we obtain

$$Z(\eta) = V^N \left(1 - 4\pi\sigma^2 \frac{N(N-1)}{2V}\right) \simeq V^N \underbrace{\exp\left[-2(N-1)\eta\right]}_{p_{\mathrm{accept}}(\eta)}. \qquad (2.8)$$

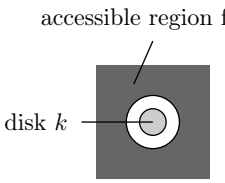

Fig. 2.22 Excluded and accessible regions for two disks of radius σ.

This implies that the probability for randomly chosen disks k and l not to overlap,

$$\left\{\begin{array}{c}\text{probability that} \\ \text{disks } k \text{ and } l \\ \text{do not overlap}\end{array}\right\} = 1 - \frac{4\pi\sigma^2}{V} \simeq \exp\left(-\frac{4\pi\sigma^2}{V}\right), \qquad (2.9)$$

is uncorrelated at low density. For 16 disks, the function in eqn (2.8) yields $p_{\mathrm{accept}} = Z(\eta)/V^N \simeq \mathrm{e}^{-30\eta}$. This fits very well the empirical acceptance rate obtained from Alg. 2.8 (`direct-disks-any`). At low density, it is exact (see Fig. 2.21).

We have computed in eqn (2.8) the second virial coefficient B of the hard-disk gas in two dimensions, the first correction term in $1/V$ beyond the ideal-gas expression for the equation of state:

$$\frac{PV}{NRT} = \frac{V}{N}\frac{\partial \log Z}{\partial V} = 1 + B\frac{1}{V} + C\frac{1}{V^2} + \cdots,$$

which, from eqn (2.8), where $\eta = \pi\sigma^2 N/V$, is equal to

$$1 + \underbrace{2(N-1)\pi\sigma^2}_{B}\frac{1}{V}.$$

This is hardly a state-of-the-art calculation in the twenty-first century, given that in 1874, Boltzmann had already computed the fourth virial coefficient, the coefficient of V^{-3} in the above expansion, for three-dimensional spheres. The virial expansion was once believed to give systematic access to the thermodynamics of gases and liquids at all densities up to close packing, in the same way that, say, the expansion of the exponential function $\mathrm{e}^x = 1 + x + x^2/2! + x^3/3! + \cdots$ converges for all real and complex x, but it becomes unwieldy at higher orders. More fundamentally, this perturbation approach cannot describe phase

transitions: there is important physics beyond virial expansions around $\eta = 0$, and beyond the safe harbor of direct-sampling algorithms.

The relation between our algorithms and the partition functions of statistical mechanics holds even for the Markov-chain algorithm in Subsection 2.2.3, which concentrates on a physical system in a small window corresponding to the throwing range. This algorithm thus overcomes the direct-sampling algorithm's limitation to low densities or small particle numbers, but has difficulties coping with large-scale structures, which no longer allow cutting up into small systems.

2.2.3 Markov-chain hard-sphere algorithm

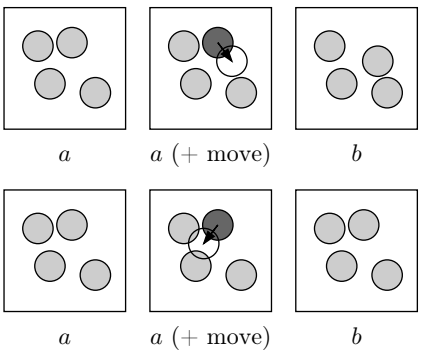

Fig. 2.23 Accepted (*top*) and rejected (*bottom*) Monte Carlo moves for a hard-disk system.

Direct sampling for hard disks works only at low densities and small particle numbers, and we thus switch to a more general Markov-chain Monte Carlo algorithm (see Alg. 2.9 (`markov-disks`)). Disks are moved

procedure `markov-disks`
input $\{\mathbf{x}_1, \ldots, \mathbf{x}_N\}$ (configuration a)
$k \leftarrow \mathtt{nran}\,(1, N)$
$\delta\mathbf{x}_k \leftarrow \{\mathtt{ran}\,(-\delta, \delta)\,, \mathtt{ran}\,(-\delta, \delta)\}$
if (disk k can move to $\mathbf{x}_k + \delta\mathbf{x}_k$**)** $\mathbf{x}_k \leftarrow \mathbf{x}_k + \delta\mathbf{x}_k$
output $\{\mathbf{x}_1, \ldots, \mathbf{x}_N\}$ (configuration b)

Algorithm 2.9 `markov-disks`. Generating a hard-disk configuration b from configuration a using a Markov-chain algorithm (see Fig. 2.23).

analogously to the way adults wander between pebble positions on the Monaco heliport, and attempts to reach illegal configurations with overlaps are rejected (see Fig. 2.23). Detailed balance between configurations holds for the same reason as in Alg. 1.2 (`markov-pi`). The Markov-chain hard-disk algorithm resembles the adults' game on the heliport (see

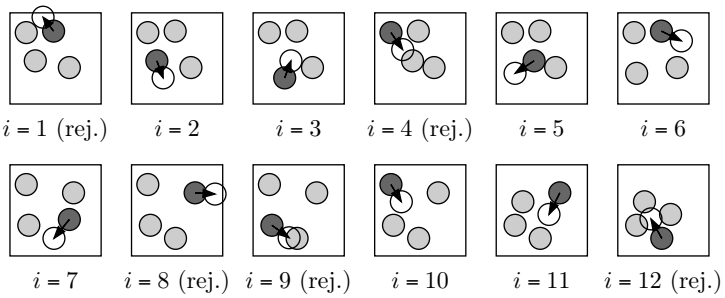

Fig. 2.24 Markov-chain Monte Carlo algorithm for hard disks in a box without periodic boundary conditions (see Alg. 2.9 (`markov-disks`)).

Fig. 2.24), but although we again drive disks (pebbles) across a two-dimensional box (the landing pad), the $2N$-dimensional configuration space is not at all easy to characterize. We must, for example, understand whether the configuration space is simply connected, so that any configuration can be reached from any other by moving disks, one at a time, with an infinitesimal step size. Simple connectivity of the configuration space implies that the Monte Carlo algorithm is ergodic, a crucial requirement. Ergodicity, in the sense just discussed, can indeed be broken for small N or for very high densities, close to jammed configurations (see the discussion of jamming in Chapter 7). For our present purposes, the question of ergodicity is best resolved within the constant-pressure ensemble, where the box volume may fluctuate (see Subsection 2.3.4), and the hard-sphere Markov-chain algorithm is trivially ergodic.

The Markov-chain algorithm allows us to generate independent snapshots of configurations for impressively large system sizes, and at high density. These typical configurations are liquid-like at low and moderate densities, but resemble a solid beyond a phase transition at $\eta \simeq 0.70$. This transition was discovered by Alder and Wainwright (1957) using the molecular dynamics approach of Section 2.1. This was very surprising because, in two dimensions, a liquid–solid transition was not expected to exist. A rigorous theorem (Mermin and Wagner 1966) even forbids positional long-range order for two-dimensional systems with short-range interactions, a class to which hard disks belong. An infinitely large system thus cannot have endless patterns of disks neatly aligned as in the right frame of Fig. 2.25. Nevertheless, in two dimensions, long-range order is possible for the orientation of links between neighbors, that is, the angles, which are approximately $0, 60, 120, 180$, and 240 degrees in the right frame of Fig. 2.25, can have long-range correlations across an infinite system. A detailed discussion of crystalline order in two dimensions would go beyond the scope of this book, but the transition itself will be studied again in Subsection 2.4, in the constant-pressure ensemble.

It is interesting to interpret the changes in the configuration space when the system passes through the phase transition. Naively, we would

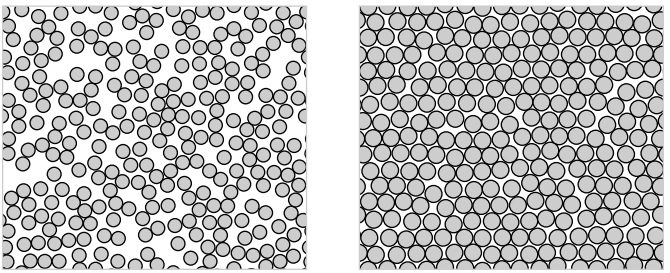

Fig. 2.25 Snapshots of 256 hard disks in a box of size $1 \times \sqrt{3}/2$ with periodic boundary conditions (from Alg. 2.9 (`markov-disks`)).

suppose that below the critical density only liquid-like configurations exist, and above the transition only solid ones. This first guess is wrong at low density because a crystalline configuration at high density obviously also exists at low density; it suffices to reduce the disk radii. Disordered configurations (configurations without long-range positional or orientational order) also exist right through the transition and up to the highest densities; they can be constructed from large, randomly arranged, patches of ordered disks. Liquid-like, disordered configurations and solid configurations of disks thus do not disappear as we pass through the liquid–solid phase transition density one way or the other; it is only the balance of statistical weights which is tipped in favor of crystalline configurations at high densities, and in favor of liquid configurations at low densities.

The Markov-chain hard-disk algorithm is indeed very powerful, because it allows us to sample configurations at densities and particle numbers that are far out of reach for direct-sampling methods. However, it slows down considerably upon entering the solid phase. To see this in a concrete example, we set up a particular tilted initial condition for a long simulation with Alg. 2.9 (`markov-disks`) (see Fig. 2.26). Even 25 billion moves later, that is, one hundred million sweeps (attempted moves per disk), the initial configuration still shows through in the state of the system. A configuration independent of the initial configuration has not yet been sampled.

We can explain—but should not excuse—the slow convergence of the hard-disk Monte Carlo algorithm at high density by the slow motion of single particles (in the long simulation of Fig. 2.26, the disk k has only moved across one-quarter of the box). However, an equilibrium Monte Carlo algorithm is not meant to simulate time evolution, but to generate, as quickly as possible, configurations a with probability $\pi(a)$ for all a making up the configuration space. Clearly, at a density $\eta = 0.72$, Alg. 2.9 (`markov-disks`) fails at this task, and Markov-chain sampling slows down dangerously.

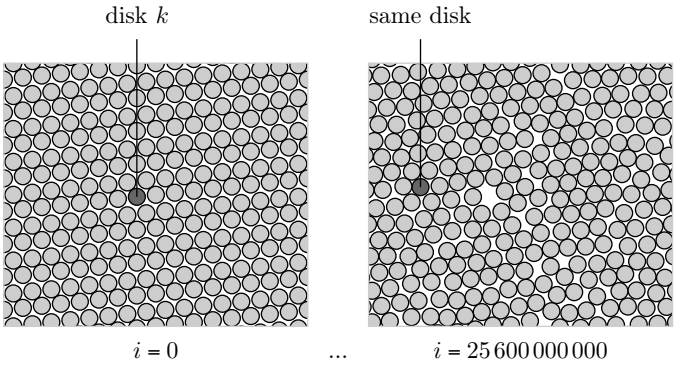

Fig. 2.26 Initial and final configurations of a Monte Carlo simulation for 256 disks (size $1 \times \sqrt{3}/2$, periodic boundary conditions, $\eta = 0.72$).

2.2.4 Velocities: the Maxwell distribution

Molecular dynamics concerns positions and velocities, whereas Alg. 2.7 (`direct-disks`) and Alg. 2.9 (`markov-disks`), only worry about positions. Why the velocities disappear from the Monte Carlo programs deserves a most thorough answer (and is a No. 1 exam question).

To understand velocities in statistical mechanics, we again apply the equiprobability principle, not to particle positions within a box, but to the velocities themselves. This principle calls for all legal sets of hard-sphere velocities to appear with the same probability:

$$\pi(\mathbf{v}_1, \ldots, \mathbf{v}_N) = \begin{cases} 1 & \text{if velocities legal} \\ 0 & \text{if forbidden} \end{cases} .$$

For concreteness, we consider hard disks in a box. A set $\{\mathbf{v}_1, \ldots, \mathbf{v}_N\}$ of velocities is legal if it corresponds to the correct value of the kinetic energy

$$E_{\text{kin}} = \frac{1}{2} m \cdot \left(\mathbf{v}_1^2 + \cdots + \mathbf{v}_N^2\right) \quad \text{(fixed)}.$$

Each squared velocity in this equation has two components, that is, $\mathbf{v}_k^2 = \mathbf{v}_{x,k}^2 + \mathbf{v}_{y,k}^2$, and any legal set of velocities corresponds to a point on a $2N$-dimensional sphere with $r^2 = 2E_{\text{kin}}/m$. The equiprobability principle thus calls for velocities to be random vectors on the surface of this $2N$-dimensional sphere (see Fig. 2.27).

We recall from Subsection 1.2.6 that random points on the surface of a hypersphere can be sampled with the help of $2N$ independent Gaussian random numbers. The algorithm involves a rescaling, which becomes unnecessary in high dimensions if the Gaussians' variance is chosen correctly (see the discussion of Alg. 1.22 (`direct-surface`)). In our case, the correct scaling is

$$\pi(v_x) = \frac{1}{\sqrt{2\pi}\sigma} \exp\left(-\frac{v_x^2}{2\sigma^2}\right), \quad \text{etc.},$$

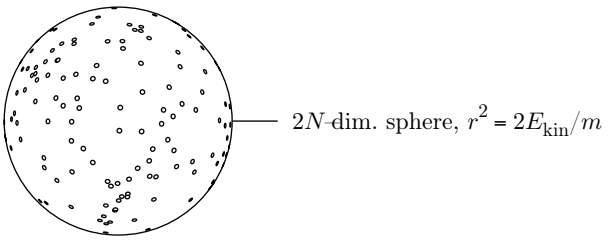

Fig. 2.27 Legal sets of velocities for N hard disks in a box.

where

$$\sigma = \sqrt{\frac{2}{m}\frac{E_{\rm kin}}{dN}}.$$

This is the Maxwell distribution of velocities in d dimensions; $E_{\rm kin}/(dN)$ is the mean kinetic energy per degree of freedom and is equal to $\frac{1}{2}k_{\rm B}T$, where T is the temperature (in kelvin), and $k_{\rm B}$ is the Boltzmann constant. We find that the variance of the Gaussian describing the velocity distribution function is $\sigma^2 = k_{\rm B}T/m$, and we finally arrive at the following expressions for the probability distribution of a single component of the velocity:

$$\pi(v_x)\,{\rm d}v_x = \sqrt{\frac{m}{2\pi k_{\rm B}T}}\exp\left(-\frac{1}{2}\frac{mv_x^2}{k_{\rm B}T}\right){\rm d}v_x.$$

In two dimensions, we use the product of distributions, one for v_x, and another for v_y. We also take into account the fact that the volume element can be written as ${\rm d}v_x\ {\rm d}v_y = {\rm d}\phi\ v\,{\rm d}v = 2\pi v\,{\rm d}v$:

$$\pi(v)\,{\rm d}v = \frac{m}{k_{\rm B}T}v\exp\left(-\frac{1}{2}\frac{mv^2}{k_{\rm B}T}\right){\rm d}v.$$

In three dimensions, we do the same with $\{v_x, v_y, v_z\}$ and find

$$\pi(v)\,{\rm d}v = \sqrt{\frac{2}{\pi}}\left(\frac{m}{k_{\rm B}T}\right)^{3/2}v^2\exp\left(-\frac{1}{2}\frac{mv^2}{k_{\rm B}T}\right){\rm d}v.$$

Here v is equal to $\sqrt{v_x^2+v_y^2}$ in two dimensions and to $\sqrt{v_x^2+v_y^2+v_z^2}$ in three dimensions.

We can compare the Maxwell distribution with the molecular dynamics simulation results for four disks in a box, and check that the distribution function for each velocity component is Gaussian (see Fig. 2.28). Even for these small systems, the difference between Gaussians and random points on the surface of the hypersphere is negligible.

In conclusion—and in response to the exam question at the beginning of this subsection—we see that particle velocities drop out of the Monte

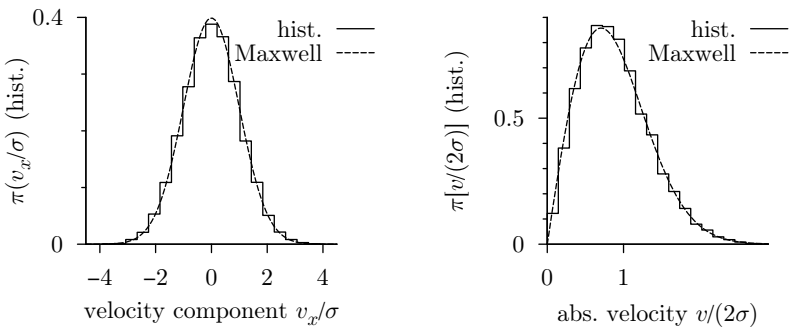

Fig. 2.28 Histograms of a velocity component v_x (*left*) and of $v = \sqrt{v_x^2 + v_y^2}$ (*right*) for four disks in a box (from Alg. 2.1 (`event-disks`)).

Carlo approach of Alg. 2.7 (`direct-disks`) and its generalizations because they form an independent sampling problem of random points on the surface of a hypersphere, solved by Alg. 1.22 (`direct-surface`), which is naturally connected to the Maxwell distribution of particle velocities.

2.2.5 Hydrodynamics: long-time tails

The direct-sampling algorithms for the positions and the velocities of hard spheres (Algs 2.7 (`direct-disks`) and 1.22 (`direct-surface`)) implement a procedure analogous to the molecular-dynamics approach, which also determines positions and velocities. In this subsection, we again scrutinize the relationship of this Monte Carlo approach to hard spheres with simulations using molecular dynamics. The theorems of Sinai and Simanyi assure us that molecular dynamics, the solution of Newton's equations, converges towards equilibrium, meaning that during an infinitely long simulation, all legal sets of positions and velocities come up with the same probability.

In a related context, concerning random processes, simple convergence towards the stationary probability distribution has proved insufficient (see Subsection 1.1.4). We needed exponential convergence, with a timescale, the correlation time, for practical equivalence of the Markov-chain approach to direct sampling. This timescale was provided by the second largest eigenvalue of the transfer matrix and it allowed us to distinguish between short and long simulations: a Markov chain that had run several times longer than the correlation time could be said to be practically in equilibrium.

As we shall see, the molecular dynamics of hard disks and spheres lacks an analogous timescale, that is, a typical time after which Alg. 2.1 (`event-disks`) would move from one set of positions and velocities to another independent set. Convergence is guaranteed by theorems in math-

ematics, but it is not exponential. The inescapable consequence of this absence of a scale is that statistical mechanics cannot capture all there is to molecular dynamics. Another discipline of physics, hydrodynamics, also has its word to say here.

We shall follow this discussion using a special quantity, the velocity autocorrelation function, whose choice we shall first describe the motivation for. We imagine a configuration of many hard disks, during a molecular dynamics simulation, in equilibrium from time $t' = 0$ to time t. Each particle moves from position $\mathbf{x}(0)$ to $\mathbf{x}(t)$, where

$$\mathbf{x}(t) - \mathbf{x}(0) = \int_0^t \mathrm{d}t' \ \mathbf{v}(t')$$

(we omit particle indices in this and the following equations). We may average this equation over all possible initial conditions, but it is better to first square it to obtain the mean squared particle displacement

$$\left\langle (\mathbf{x}(t) - \mathbf{x}(0))^2 \right\rangle = \int_0^t \mathrm{d}t' \ \int_0^t \mathrm{d}t'' \ \underbrace{\left\langle (\mathbf{v}(t') \cdot \mathbf{v}(t'')) \right\rangle}_{C_{\mathbf{v}}(t''-t')}.$$

For a rapidly decaying velocity autocorrelation function, the autocorrelation function $C_{\mathbf{v}}$ will be concentrated in a strip around $\tau = t'' - t' = 0$ (see Fig. 2.29). In the limit $t \to \infty$, we can then extend the integration, as shown, let the strip extension go to ∞, and obtain the following, where $\tau = t'' - t'$:

$$\frac{1}{t} \left\langle (\mathbf{x}(t) - \mathbf{x}(0))^2 \right\rangle \simeq \frac{1}{t} \underbrace{\iint}_{\substack{\text{strip in} \\ \text{Fig. 2.29}}} \mathrm{d}t' \ \mathrm{d}\tau \ C_{\mathbf{v}}(\tau)$$

$$\xrightarrow[\substack{\text{decay of } C(\tau) \\ \text{faster than } 1/\tau}]{t\to\infty} 2 \int_0^\infty \mathrm{d}\tau \ C_{\mathbf{v}}(\tau) = 2D, \quad (2.10)$$

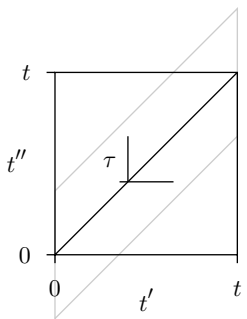

Fig. 2.29 Integration domain for the velocity autocorrelation function (*square*), and strip chosen (*gray*), equivalent for $t \to \infty$.

We see that the mean square displacement during the time interval from 0 to t is proportional to t (not to t^2, as for straight-line motion). This is a hallmark of diffusion, and D in the above equation is the diffusion constant. Equation (2.10) relates the diffusion constant to the integrated velocity autocorrelation function. Exponential decay of the autocorrelation function causes diffusive motion, at least for single particles, and would show that molecular dynamics is practically identical to statistical mechanics on timescales much larger than the correlation time.

The simple version of Alg. 2.1 (`event-disks`) (with none of the refinements sketched in Subsection 2.1.1) allows us to compute the velocity autocorrelation function in the interesting time regime for up to $\simeq 1000$ disks. It is best to measure time in units of the collision time: between time 0 and time t', each particle should have undergone on average t' collisions—the total number of pair collisions in the system should be $\simeq \frac{1}{2} N t'$. Even with a basic program that tests far more collisions than necessary, we can redo a calculation similar that of Alder and Wainwright

(1970), and produce the clear-cut result for the correlation between the velocity $\mathbf{v}_k(t)$ of particle k at time t and the velocity $\mathbf{v}_k(t+\tau)$ at some later time (see Fig. 2.30). There is no indication of an exponential decay of the autocorrelation function (which would give a timescale); instead, the velocity autocorrelation function of the two-dimensional hard-sphere gas decays as a power law $1/\tau$. In d dimensions, the result is

$$C_{\mathbf{v}}(\tau) = \langle(\mathbf{v}(0)\cdot\mathbf{v}(\tau))\rangle \propto \frac{1}{\tau^{d/2}}. \tag{2.11}$$

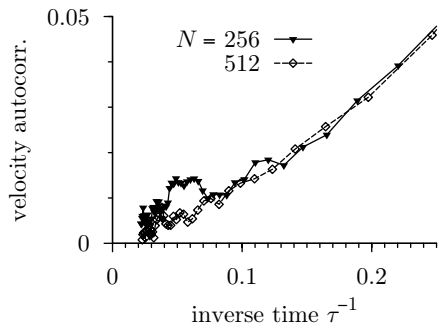

Fig. 2.30 Velocity autocorrelation for disks vs. inverse time (in collisions per disk; $\eta = 0.302$, square box, from Alg. 2.1 (`event-disks`)).

The disks in the simulation are in equilibrium: snapshots of velocities give only the Maxwell distribution. It makes sense, however, to consider the direction of motion of a particle during a certain time interval. In order to move in that direction, a particle has to get other particles (in front of it) out of the way, and these, in turn, form a kind of eddy that closes on itself behind the original particle, pushing it to continue moving in its original direction. Theoretically, long-time tails are very well understood, and detailed calculations confirm the picture of eddies and the results of straightforward molecular dynamics (for an introductory discussion of long-time tails, see Pomeau and Résibois (1975)).

Long-time tails are most pronounced in two dimensions, basically because particles that are pushed away in front of a target disk have only two directions to go. In this case, of two dimensions, this constriction has dangerous effects on the diffusion constants: the mean square displacement, for large time intervals t, is not proportional to t as in diffusive motion, but to $t \log t$. (This follows from entering eqn (2.11) into eqn (2.10).) All this, however, does not imply that, in two dimensions, diffusive motion does not exist and that, for example, a colloidal Brownian particle on a water surface in a big shallow trough moves faster and faster as time goes on. For very slow motion, thermal coupling to the outside world restores a finite diffusion constant (for an example of thermal coupling, see Subsection 2.3.1). It is certainly appropriate to treat